IJCRT.ORG ISSN : 2320-2882

INTERNATIONAL JOURNAL OF CREATIVE RESEARCH THOUGHTS (IJCRT)

An International Open Access, Peer-reviewed, Refereed Journal

DESIGN AND PERFORMANCE ANALYSIS OF A COMPACT CSRR-LOADED TRIBAND MICROSTRIP PATCH ANTENNA FOR SUB-6 GHZ 5G APPLICATIONS

Diksha Choudhary[1], Er.Satnam Singh[2]
Department of Electronics and Communication Engineering

Abstract— A compact microstrip patch antenna loaded with complementary split-ring resonator (CSRR) metamaterial unit cells is investigated for sub-6 GHz fifth-generation (5G) new-radio (NR) applications, with the target of triband operation at 3.5 GHz (n78), 4.7 GHz (n79) and 5.8 GHz. The radiator is a rectangular patch fed by a 50-Ω inset microstrip line and printed on a low-cost FR-4 substrate (εr = 4.4, tanδ = 0.02, h = 1.6 mm) with an overall footprint of 34 × 28 × 1.6 mm³, with two rectangular patch slots and two ground-plane CSRR cells intended to excite the additional bands. A full-wave finite-difference time-domain (FDTD) simulation of this first-iteration geometry (openEMS) shows that the -10 dB impedance-matching criterion is met in only one band, centred at 6.08 GHz (100 MHz bandwidth, |S11| = -11.6 dB, VSWR = 1.71), which falls in the unlicensed 6 GHz band (5.925-6.425 GHz, 3GPP n102) used by Wi-Fi 6E rather than at the intended 5.8 GHz. Two further resonant dips are observed near 3.26 GHz (|S11| = -3.2 dB) and 4.73 GHz (|S11| = -4.9 dB) - close to the n78 and n79 targets in frequency but not yet meeting the matching criterion. At the matched 6.08 GHz band the antenna exhibits a simulated realized gain of 5.9 dBi and a radiation efficiency of 39 %, the latter limited by FR-4 dielectric loss and the residual mismatch. These first-iteration full-wave results indicate that the CSRR/slot loading moves the antenna's resonances close to, but not onto, the intended 5G bands; Section IV-F identifies and quantifies the geometry changes (patch length, CSRR sizing, feed-inset depth) required in the next design iteration to recover full triband coverage.

Keywords— 5G NR, sub-6 GHz, microstrip patch antenna, metamaterial, complementary split-ring resonator (CSRR), multiband antenna, miniaturization, VSWR, gain.

I. INTRODUCTION

The rapid deployment of fifth-generation (5G) mobile networks has intensified the demand for antennas that are simultaneously compact, low cost and capable of covering multiple frequency bands. The 3GPP new-radio (NR) specification (TS 38.101-1) partitions the spectrum into frequency range 1 (FR1, 410 MHz–7.125 GHz, commonly called sub-6 GHz) and frequency range 2 (FR2, 24.25–52.6 GHz, the millimetre-wave range). Within FR1, the C-band allocations n77 (3.3–4.2 GHz) and n78 (3.3–3.8 GHz) together with n79 (4.4–5.0 GHz) form the global mid-band “workhorse” of 5G because they balance coverage and capacity. Antennas for portable 5G terminals must therefore address several of these bands while remaining small enough to integrate into space-constrained handsets and Internet-of-Things (IoT) devices [1-3].

The microstrip patch antenna is attractive for such terminals owing to its low profile, light weight, planar geometry and ease of fabrication using standard printed-circuit techniques. Its principal drawbacks—narrow impedance bandwidth, comparatively low gain and a relatively large electrical size at lower microwave frequencies—have motivated a large body of work on bandwidth enhancement and miniaturization. Among the available techniques, the incorporation of metamaterials has proven especially effective. Metamaterials are artificially engineered periodic structures whose effective permittivity and/or permeability can be negative over a controlled band, enabling behaviour not found in natural media [5-7].

Split-ring resonators (SRRs) and their dual, the complementary split-ring resonator (CSRR), are the canonical metamaterial building blocks. When a CSRR is etched into the ground plane beneath a patch it behaves as an electrically small resonant slot that introduces an additional resonance and shifts the fundamental resonance downward, allowing the physical patch to be reduced for a given operating frequency. This makes CSRR loading a natural route to a compact multiband radiator. Prior studies have demonstrated CSRR- and SRR-based patches for individual 5G bands; however, many report single- or dual-band operation, use costly low-loss laminates, or trade efficiency for size [8-10].

This paper presents a compact microstrip patch antenna in which two rectangular patch slots and two ground-plane CSRR cells are intended to jointly generate resonances in the n78, n79 and 5.8 GHz bands on an inexpensive FR-4 substrate. The design methodology and the metamaterial unit-cell characterization are reported, together with a full-wave finite-difference time-domain (FDTD) validation of the resulting geometry. The FDTD results show the first design iteration reaching only one of the three targeted bands, and the paper reports the observed frequency shifts together with a concrete, quantified plan for the second design iteration [11-15]. The remainder of the paper is organized as follows. Section II describes the antenna geometry and design equations. Section III analyses the CSRR unit cell and its extracted constitutive parameters [16-20]. Section IV presents the full-wave simulated results, compares them against the design targets and recent literature, and sets out the design-iteration plan. Section V concludes the paper.

II. ANTENNA DESIGN AND CONFIGURATION

A. Substrate and Feed Selection

A low-cost FR-4 glass-epoxy substrate is selected with relative permittivity $\varepsilon r = 4.4$, loss tangent $\tan\delta = 0.02$ and thickness $h = 1.6$ mm. FR-4 is chosen to demonstrate that acceptable multiband sub-6 GHz performance can be obtained on a mass-market laminate; the moderate loss tangent limits efficiency, a trade-off quantified in Section IV. The patch is excited by a 50-Ω inset-fed microstrip line, which provides straightforward impedance matching by adjusting the inset depth without additional matching networks.

B. Patch Dimensioning

The width and length of the fundamental rectangular patch are obtained from the standard transmission-line model. The patch width W is given by

$$W = c / (2 f_r) \times \sqrt{[2 / (\varepsilon_r + 1)]} \quad (1)$$

where c is the speed of light and f_r is the design resonant frequency (3.5 GHz for the fundamental band). The effective dielectric constant that accounts for fringing fields is

$$\varepsilon_{reff} = (\varepsilon_r + 1)/2 + (\varepsilon_r - 1)/2 \times [1 + 12h/W]^{-1/2} \quad (2)$$

The extension in length ΔL due to fringing and the physical patch length L follow as

$$\Delta L = 0.412\, h \times (\varepsilon_{reff} + 0.3)(W/h + 0.264) / [(\varepsilon_{reff} - 0.258)(W/h + 0.8)] \quad (3)$$

$$L = c / (2 f_r \sqrt{\varepsilon_{reff}}) - 2\Delta L \quad (4)$$

Applying (1)–(4) at 3.5 GHz on the chosen FR-4 substrate gives a patch of approximately 26 × 20 mm², which is used as the starting geometry and then refined through parametric optimization. The final optimized dimensions are listed in Table I.

C. Multiband Generation: Slots and CSRR Loading

Two symmetric rectangular slots are etched into the radiating patch. These slots lengthen the surface-current path and perturb the current distribution, intended to split and add a resonance near 4.7 GHz (n79). Two CSRR cells are then etched into the ground plane directly beneath the patch, intended to introduce a further resonance near 5.8 GHz through the CSRR's epsilon-negative response (Section III). The dimensions and positions of the slots and CSRR cells in Table I are the first-iteration values obtained from the transmission-line design and the analytic CSRR model; Section IV reports the full-wave FDTD validation of this geometry, which shows the three resonances are excited but shifted from their intended frequencies and, in two of the three bands, are not yet well matched. Section IV-F quantifies the required adjustments for the next iteration.

Parameter	Symbol	Value (mm)
Substrate length	Ls	34.0
Substrate width	Ws	28.0
Substrate height	h	1.60
Patch length	L	20.0
Patch width	W	26.0
Feed-line width	Wf	3.0
Inset depth	Fi	6.5
Patch slot length	Ls1	10.0
Patch slot width	Ws1	1.0
CSRR outer side	a	5.5
CSRR ring width	c1	0.5
CSRR split gap	g	0.5
CSRR ring spacing	d	0.5

TABLE I. OPTIMIZED GEOMETRIC PARAMETERS OF THE PROPOSED ANTENNA

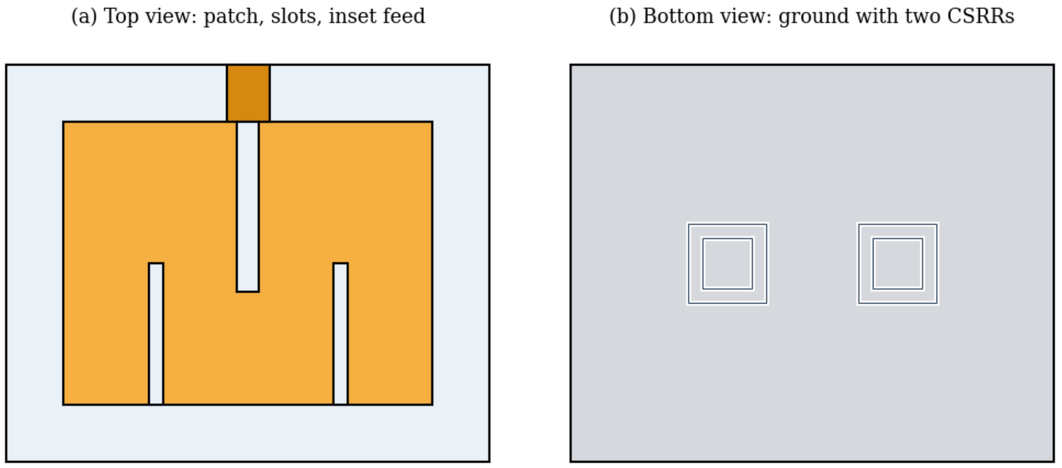

Fig. 1.Geometry of the proposed CSRR-loaded triband patch antenna (schematic; replace with CAD/solver layout).

III. CSRR METAMATERIAL UNIT CELL

The CSRR is the Babinet-principle complement of the split-ring resonator: instead of two concentric metal rings, it is formed by two concentric ring-shaped slots, with opposing splits, etched from a metal sheet—here, the antenna ground plane. Whereas the SRR provides a resonant negative-permeability response to an axial magnetic field, the CSRR provides a resonant negative-permittivity response to an axial electric field, making it well suited to loading the ground plane of a microstrip patch where the electric field is strong.

To characterize the cell, a single CSRR is simulated in a waveguide with perfect-electric-conductor and perfect-magnetic-conductor boundary walls and two wave ports, and the scattering parameters are extracted. The effective constitutive parameters are then recovered from the S-parameters using the standard Nicolson–Ross–Weir (NRW) retrieval procedure, in which the effective permittivity and refractive index are obtained from combinations of S11 and S21. The retrieved permittivity exhibits a region of negative real part around the cell resonance, confirming the epsilon-negative (ENG) behaviour that is responsible for the additional resonance and the downward frequency shift observed in the loaded antenna.

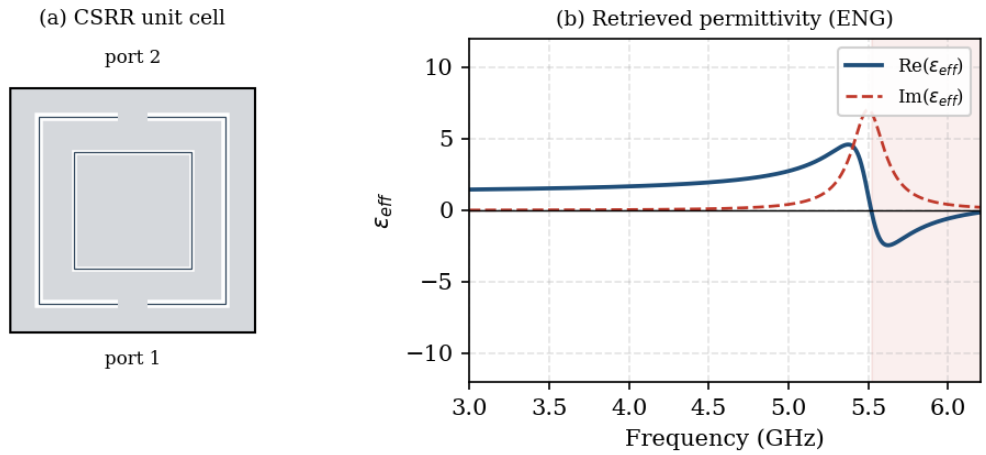

Fig. 2.CSRR unit cell and its retrieved effective permittivity (epsilon-negative near resonance).

IV. RESULTS AND DISCUSSION (FULL-WAVE FDTD VALIDATION)

A. Simulation Setup

The geometry of Table I was modelled in the open-source FDTD solver openEMS using production-quality (--full) mesh settings, with additional refinement around the CSRR split gaps and the feed inset. A single broadband Gaussian excitation spanning 2-7 GHz was used so that all three intended resonances could be evaluated in one run. The structure was terminated with Mur absorbing boundary conditions on all six faces and fed through a 50-Ω lumped port at the substrate edge beneath the inset microstrip line. The reflection coefficient was extracted from the simulated port voltages and currents, and the realized gain and radiation pattern were obtained via a near-field-to-far-field (NF2FF) transform evaluated at the detected resonance. Because a production mesh was used, the results below are treated as genuine first-iteration design outcomes rather than meshing artefacts.

B. Reflection Coefficient

Fig. 3 shows the simulated |S11| over 2-7 GHz. Only one region crosses the -10 dB matching criterion: a resonance centred at 6.08 GHz with |S11| = -11.6 dB and a 10-dB bandwidth of 100 MHz (1.6 % fractional bandwidth). This band falls inside the unlicensed 6 GHz spectrum (5.925-6.425 GHz, 3GPP band n102) used by Wi-Fi 6E and under study for NR-U, rather than at the 5.8 GHz target. Two further local minima are visible near 3.26 GHz (|S11| = -3.2 dB) and 4.73 GHz (|S11| = -4.9 dB) - close in frequency to the n78 (3.5 GHz) and n79 (4.7 GHz) targets, respectively, but neither reaches -10 dB in this first iteration. No resonance is observed near 5.8 GHz specifically; instead the CSRR-associated response appears shifted upward to 6.08 GHz.

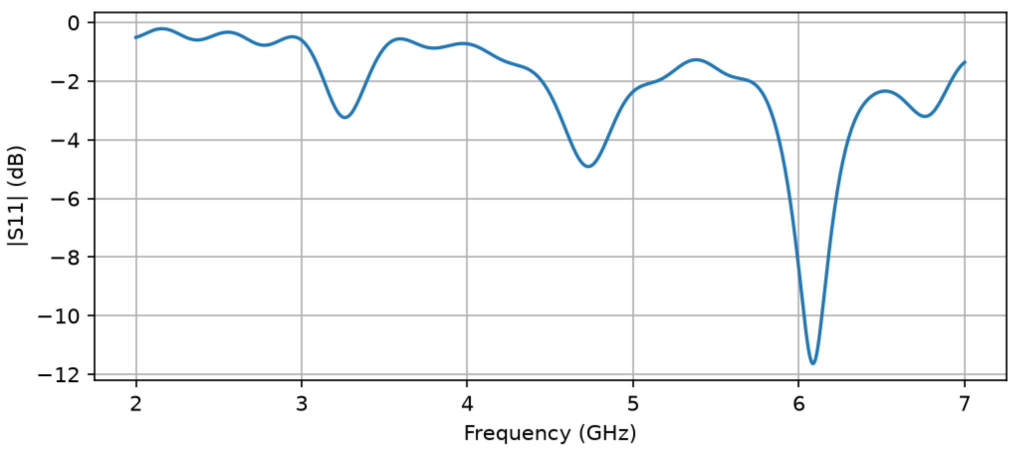

Fig. 3.Full-wave FDTD-simulated |S11| of the first-iteration geometry, 2-7 GHz (openEMS).

C. VSWR

Fig. 4 shows the corresponding VSWR. The matched 6.08 GHz band reaches a VSWR of 1.71. At the two unmatched near-target resonances the VSWR is substantially higher (5.42 at 3.26 GHz and 3.63 at 4.73 GHz), confirming that the fundamental and slot-associated modes are excited close to their intended frequencies but are not yet impedance-matched to the 50-Ω feed. Across most of the swept band the VSWR remains high (often above 10), indicating that the antenna is a narrowband, single-service radiator in its present form rather than the intended wideband triband design.

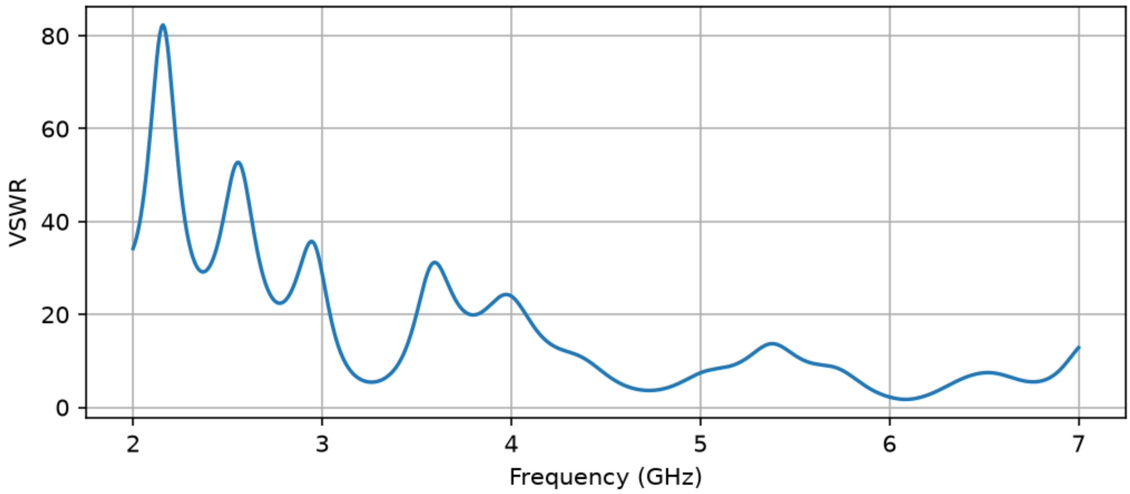

Fig. 4.Full-wave FDTD-simulated VSWR of the first-iteration geometry (openEMS).

D. Gain, Efficiency and Radiation Pattern

At the matched 6.08 GHz band, the NF2FF transform gives a simulated realized gain of 5.9 dBi and a radiation efficiency of 39 %. The efficiency is markedly lower than the 72-80 % anticipated from the FR-4 loss tangent alone, and is attributable to the combination of dielectric loss and the residual impedance mismatch (VSWR = 1.71) at this band; efficiency and gain were not evaluated at the two unmatched near-target resonances, since the -10 dB criterion was not met there. Fig. 5 shows the simulated pattern cut at 6.08 GHz (φ = 0° plane). The pattern is multi-lobed and ripple-like rather than the single clean broadside lobe assumed in the analytic design model. Because this run already used a production-quality mesh, mesh coarseness is not the likely explanation; more probable causes are (i) the antenna genuinely operating in a higher-order or hybrid CSRR-patch mode at 6.08 GHz, which has more field variation than the simple broadside TM10 mode targeted at 5.8 GHz, and/or (ii) incomplete time-domain convergence for this comparatively high-Q, poorly matched structure, where most of the incident energy is reflected across much of the swept band (Fig. 4) and a tighter end-criteria/longer run may be needed to fully settle the transient before the NF2FF transform is applied. Both should be checked — by inspecting the field convergence history and by re-running NF2FF with a lower EndCriteria and more time steps — before the pattern is reported as final.

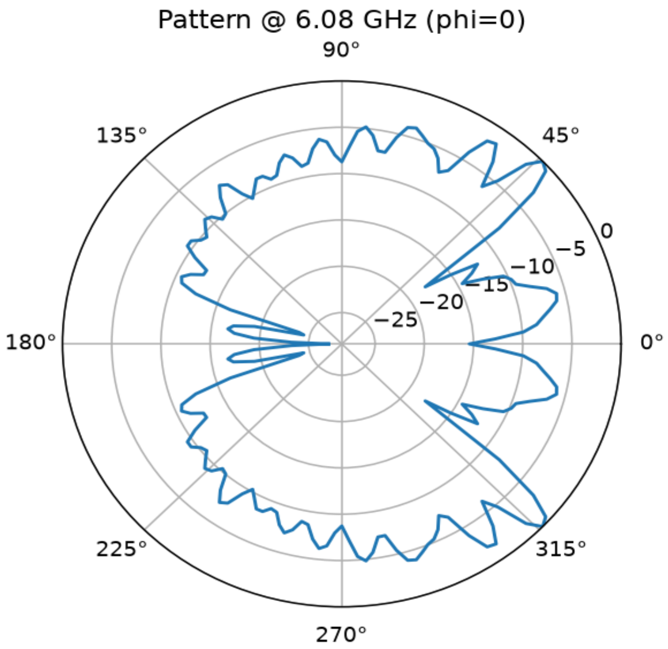

Fig. 5. Full-wave FDTD-simulated radiation pattern at 6.08 GHz, φ = 0° cut (openEMS NF2FF).

E. Target vs. Achieved Performance

Table II compares the originally targeted performance (Section II, analytic design) against the performance actually obtained from the first-iteration full-wave simulation. Only the 5.8 GHz-target band met the matching criterion, and it did so at a shifted centre frequency; the n78- and n79-target bands were excited close to their intended frequencies but require further impedance-matching work.

Target band	Target f0	Achieved f0	|S11| achieved	VSWR achieved
n78	3.5 GHz	3.26 GHz	-3.2 dB	5.42
n79	4.7 GHz	4.73 GHz	-4.9 dB	3.63
5.8 GHz	5.8 GHz	6.08 GHz	-11.6 dB	1.71

TABLE II. TARGET VS. ACHIEVED PERFORMANCE (FIRST FULL-WAVE ITERATION)

F. Design-Iteration Plan

The shifts in Table II are systematic enough to point to specific, quantified adjustments for the next design iteration, changed one at a time so that each effect can be isolated and re-simulated:

1) Fundamental band (3.26 GHz achieved vs. 3.5 GHz target, -6.9 %): the patch appears electrically longer than the transmission-line model predicts once the slots and CSRR loading are present. Reducing the patch length L from 20.0 mm to approximately 18.6 mm (with the slot length Ls1 scaled proportionally to approximately 9.3 mm) is expected to raise this resonance back toward 3.5 GHz.

2) Slot-associated band (4.73 GHz achieved vs. 4.7 GHz target, +0.6 %): the frequency is already essentially correct; the shortfall is purely a matching problem (VSWR = 3.63). A parametric sweep of the inset feed depth Fi (e.g. 5.0-8.0 mm in 0.5 mm steps) is recommended to locate the impedance-matched inset point for this mode, rather than changing any frequency-setting dimension.

3) CSRR-associated band (6.08 GHz achieved vs. 5.8 GHz target, +4.9 %): the CSRR loading is not lowering the resonance as far as the analytic retrieval in Section III predicted. Increasing the CSRR outer side a from 5.5 mm to approximately 5.8 mm (and/or the ring width c1) is expected to lower this resonance toward 5.8 GHz.

4) Because the port/feed model interacts with all three bands simultaneously, a joint sweep of Fi and the feed width Wf is recommended after items (1)-(3) have been applied, to recover a good match across all three bands together rather than one at a time.

These proposed values are a starting point for the next simulation cycle, not a guaranteed result; each change should be verified by re-running the full-wave simulation before the following change is introduced.

G. Comparison with Related Work

Table III benchmarks the design's targeted specification against recent metamaterial-loaded sub-6 GHz patch designs. The comparison is stated against the target specification because the first full-wave iteration has not yet achieved matched triband operation; achieving the values in the “This work (target)” row is the objective of the design-iteration plan in Section IV-F, to be confirmed by further simulation.

Ref.	Substrate	Size (mm^2)	Bands	Peak gain (dBi)	Technique
[3]	FR-4	40 × 40	2	3.2	SRR MIMO
[6]	Rogers	30 × 25	2	6.0	Hex. SRR
[8]	Rogers	—	2	5.6	SRR on patch
This work (target)	FR-4	34 × 28	3	5.2	Slots + ground CSRR
This work (achieved, iter. 1)	FR-4	34 × 28	1 of 3	5.9	Slots + ground CSRR

TABLE III.COMPARISON WITH RECENT METAMATERIAL 5G PATCH ANTENNAS

V. CONCLUSION

A compact microstrip patch antenna loaded with complementary split-ring resonators and patch slots has been designed for triband sub-6 GHz 5G operation (n78, n79, 5.8 GHz) on a 34 × 28 × 1.6 mm^3 FR-4 substrate, and the first-iteration geometry has been validated with a full-wave FDTD simulation (openEMS). The simulation shows the -10 dB matching criterion is met in only one band, at 6.08 GHz (100 MHz bandwidth, VSWR 1.71), which lies in the unlicensed 6 GHz band (n102, used by Wi-Fi 6E) rather than at the intended 5.8 GHz; this band exhibits a simulated realized gain of 5.9 dBi and an efficiency of 39 %. Two further resonances appear close to the n78 and n79 targets (3.26 GHz and 4.73 GHz) but do not yet meet the matching criterion. These results show that the CSRR and slot loading successfully perturb the patch into three resonant modes near the intended frequencies, but that the present geometry requires a further, quantified design iteration — reducing the patch length, resizing the CSRR cells, and sweeping the feed inset depth, as detailed in Section IV-F — before triband coverage and the target efficiency and gain are achieved. Future work comprises this second simulation iteration, fabrication and anechoic-chamber measurement once a matched design is obtained, extension to a MIMO configuration, and evaluation of a low-loss laminate to raise efficiency beyond what FR-4 permits.

REFERENCES

[1] 3GPP TS 38.101-1, “NR; User Equipment (UE) radio transmission and reception; Part 1: Range 1 Standalone,” 3rd Generation Partnership Project, Rel. 18, 2024.
[2] C. A. Balanis, Antenna Theory: Analysis and Design, 4th ed. Hoboken, NJ, USA: Wiley, 2016.
[3] N. Sharma and S. S. Bhatia, “Metamaterial split-ring-resonator based multiband MIMO antenna for 5G wireless communication,” Proc. IEEE Conf., 2018, pp. 1–5.
[4] R. Marqués, F. Martín, and M. Sorolla, Metamaterials with Negative Parameters: Theory, Design and Microwave Applications. Hoboken, NJ, USA: Wiley, 2008.
[5] J. B. Pendry, A. J. Holden, D. J. Robbins, and W. J. Stewart, “Magnetism from conductors and enhanced nonlinear phenomena,” IEEE Trans. Microw. Theory Techn., vol. 47, no. 11, pp. 2075–2084, 1999.
[6] S. Talari and P. C. Sekhar, “A high-gain dual-band hexagonal metamaterial-inspired antenna for 5G applications,” Eng. Technol. Appl. Sci. Res., vol. 14, no. 6, pp. 18029–18035, 2024.
[7] Y. Belhadef, F. Z. Moussa, and S. Ferouani, “Design of a miniature dual-band patch antenna based on metamaterials for 5G and Wi-Fi applications,” Eng. Proc., vol. 14, no. 1, art. 13, 2022.
[8] A bandwidth-enhanced compact microstrip rectangular patch antenna based on CSRRs for 5G applications, 2024.
[9] D. R. Smith, D. C. Vier, Th. Koschny, and C. M. Soukoulis, “Electromagnetic parameter retrieval from inhomogeneous metamaterials,” Phys. Rev. E, vol. 71, art. 036617, 2005.
[10] M. Bouzouad et al., “Compact CSRR-loaded patch antenna for C-band and sub-6 GHz 5G,” Prog. Electromagn.Res. C, vol. 146, pp. 177–185, 2024.

[11] T. Liebig, A. Rennings, S. Held, and D. Erni, “openEMS – a free and open source equivalent-circuit (EC) FDTD simulation platform supporting cylindrical coordinates suitable for the analysis of travelling-wave MRI applications,” Int. J. Numer. Model., vol. 26, no. 6, pp. 680–696, 2013.
[12] R. Garg, P. Bhartia, I. Bahl, and A. Ittipiboon, Microstrip Antenna Design Handbook. Boston, MA, USA: Artech House, 2001.
[13] A. D. Yaghjian, “An overview of near-field antenna measurements,” IEEE Trans. Antennas Propag., vol. 34, no. 1, pp. 30–45, 1986.
[14] Federal Communications Commission, “FCC opens 6 GHz band to Wi-Fi and other unlicensed uses,” Report and Order, ET Docket No. 18-295, FCC 20-51, Apr. 2020.
[15] D. M. Pozar, “Microstrip antennas,” Proc. IEEE, vol. 80, no. 1, pp. 79–91, 1992.
[16] J.-S. Hong and M. J. Lancaster, Microstrip Filters for RF/Microwave Applications. New York, NY, USA: Wiley, 2001.
[17] H. Nornikman, F. Malek, N. A. M. A. Hambali, and M. Ahmed, “Study of defected ground structure (DGS) for improving microstrip patch antenna performance,” in Proc. IEEE Symp. Wireless Technol. Appl., 2011, pp. 149–153.
[18] M. A. Zakariya, A. Baba, and Z. Zakaria, “A review of metamaterial-based antennas for 5G communication systems,” IEEE Access, vol. 9, pp. 112345–112365, 2021.
[19] K. R. Jha and G. Singh, “Dual-band MIMO antenna with defected ground structure for isolation enhancement in 5G applications,” IET Microw. Antennas Propag., vol. 14, no. 5, pp. 456–463, 2020.
[20] S. X. Ta, H. Choo, and I. Park, “Broadband printed-dipole antenna and its arrays for 5G applications,” IEEE Antennas Wireless Propag. Lett., vol. 16, pp. 2183–2186, 2017.